IIETA International Information and Engineering Technology Association
Advancing the World of Information and Engineering

Journal of New Materials for Electrochemical Systems
Vol. 23, No.1, January, 2020, pp. 7-12
http://new-mat.org
http://iieta.org/journals/jnmes

Preparation of PbS/NiO Composite Photocathode and Their Applications in Quantum Dot Sensitized Solar Cells

Shuang Liu[1,2], Lu Liu[2], Qingzhuo Du[2], Zeyuan Ma[2], Yuhang Fu[2], Yajun Zhao[2], Xiaowei Li[2] and Xiaohui Zhao[2*]

[1] College of Quality Technology Supervision, Hebei University, Baoding 071002, China
[2] Hebei Key Lab of Optic-electronic Information and Materials, College of Physics Science and Technology, Hebei University, Baoding 071002, China

Corresponding Author Email: xhzhao@hbu.edu.cn

ABSTRACT

The nanosized urchin-like NiO was synthesised by a simple hydrothermal method at high temperature, and a variety of comparative experiments were designed for studying the influence of different chemical bath deposition (CBD) cycles of PbS deposition on the photoelectric properties of quantum dot sensitized solar cells. Moreover, a novelty modified $(CH_3)_4N)_2S/((CH_3)_4N)_2S_n$ electrolyte was introduced in this solar cell successfully and NiS as the counter electrode. The result suggested that the maximum power conversion efficiency of 1.07% was obtained when after three CBD cycles of PbS, with a significantly open circuit voltage (V_{oc}) of 0.538 V, a high short circuit current density (J_{sc}) of 8.53 mA cm^{-2} and a fill factor (ff) of 0.23%.

Keywords: *oxides, electrochemical measurements, chemical synthesis, electrochemical properties*

Received: November-30-2019, Accepted: December-08-2019, https://doi.org/10.14447/jnmes.v23i1.a02

1. INTRODUCTION

Quantum dot-sensitized solar cells (QDSCs) are a promising alternative to dye-sensitized solar cells (DSCs), which attracted significantly interest in recent years due to its low cost, easy fabrication, and high theoretical power conversion efficiency [1-4]. Most QDSCs were focused primarily on the research of n-type semiconductor oxide, such as TiO_2 [5], ZnO [6], and SnO_2 [7], where photocurrents arise from photoexcited electrons injection into [8-10]. In 1999, He et al. [11] reported the first use of p-type semiconductor oxides as photocathodes in solar cells. Ever since, p-type semiconductors were increasingly further researched by a great many relevant groups. P-type photocathodes carriers transport were hole injection from the QDs into the p-type semiconductors instead of electron injection compared to n-type photoanodes [12, 13].

NiO is a most popular p-type semiconductor oxide with good stability and transparency properties for sensitized photocathodes [14, 15]. In addition, it has also been used as a photocathode material because its wide band gap from energy range from 3.6 to 4.0 eV. Combining such photocathodes with photoanodes in a tandem photoelectrochemical solar cell, whose cell voltages and theoretical efficiency would be far higher than single junction solar cell [16]. Nevertheless, the current depends on the lower current of n-type and p-type solar cell, so the high theoretical power conversion efficiency has not been realized, resulting from the fact that the current of such tandem structure systems so far been limited by the poor performance of the p-type solar cell. Photocurrent matching is essential to obtain good photoelectric conversion efficiency tandem solar cell [17]. As a result, the development and study of p-type photocathodes in the tandem structure systems might pave way for the promising photoelectric characteristic of the solar cell.

Previous studies with conventional dye-sensitized solar cells (DSCs) showed that electron transfer photoanodes were more efficient than hole injection photocathodes. One reason was that fast recombination of holes injected into the NiO VB when dye molecules reduced [18, 19]. Therefore, one approach that potentially could solve the problem was replacing the dye with inorganic semiconductor quantum dots such as CdS, CdSe, ZnS and PbS [16, 20]. Inorganic semiconductor QDs exhibits several advantages over organic dyes, such as low cost, easy obtain ability, convertibility of band gap and high molar extinction coefficient [15, 21-22]. What's more, the high extinction coefficient of semiconductor nanocrystals make light absorption improve [23], and smaller hole transport resistance for faster transport [14]. Among these nanomaterials, lead sulfide (PbS) is a promising material that has been reported to have proper band gap of about 0.8 eV in the material, which could be tuned to absorb band in the near-IR of the solar spectrum [24-26]. However, up to now, the use of PbS deposited p-type NiO photocathode in the QDSCs has not been reported.

In 2009, Rhee et al. [27] experimentally demonstrated p-type Cu_2S sensitized p-type NiO solar cell synthesised by depositing Cu_2S quantum dot on the mesoporous NiO photocathode for the first time, and open-circuit voltage of 91-95mV and short-circuit current of 260-360 mA were eventually obtained. The conversion efficiency for CdSe sensitized p-type NiO solar cells to a best report of 0.35% had been reached by Park and co-workers. In 2016, Raissi et al. [28] reported the fabrication of NiO-based QDSCs using PbS QDs with a cobalt electrolyte and Pt counter. Finally the best conversion efficiency of solar cell achieved 0.4%.

In the paper, the nanosized urchin-like NiO was prepared by a simple hydrothermal method at high temperature [29, 30]. and narrow band gap PbS quantum dots (QDs) were grown on NiO film by Chemical Bath deposition (CBD)

method [31-35]. A modified $(CH_3)_4N)_2S/((CH_3)_4N)_2S_n$ electrolyte was successfully employed in PbS QDs (Figure 1). Here we show for the first time that PbS quantum dots were deposited on NiO solar cell. To the best of our knowledge, the J_{sc} (8.53mA/cm^2) and power conversion efficiency (1.07%) are the highest values for the QD-sensitized p-type NiO solar cells.

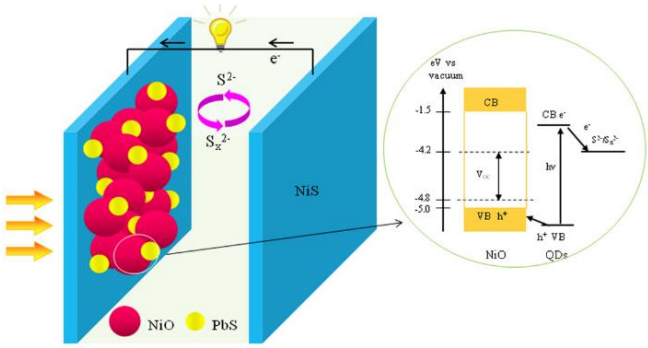

Figure 1. A schematic diagram illustrating the working principle of PbS-sensitized mesoscopic p-NiO solar cells

2. EXPERIMENTAL

2.1 Material

All compounds were purchased either from Aladdin Inc. or from Macklin Inc. Their chemical names and purities are given in Table 1.

Table 1. Materials

Chemical name	Purity, wt.%	Vendor
NiCl2·6H2O Na2S▪9H2O	99.99	Aladdin Inc.
Urea Pb(NO3)2	99	
Ethanol, methanol, thioglycolic acid, 25wt% Tetramethylammonium hydroxide methanol, 20 wt% (NH4)2S aqueous solution	-	
Ni(NO3)2·6H2O	98	
Sublimed sulfur	99.95	Macklin Inc.
3-Methoxypro-pionitrile, 4-tert-butylpyridine	98	
Lithium perchlorate	99.9	

NiCl2·6H2O (99.99%), ethanol, methanol, thioglycolic acid, Pb(NO3)2 (99%), Na2S▪9H2O (99.99%), Ni(NO3)2·6H2O (98%), Sublimed sulfur (99.95%), Tetramethylammonium hydroxide solution (25% in methanol), Ammonium sulfide solution (20% in H2O) were purchased from aladdin. 3-Methoxypro-pionitrile (98%), 4-tert-butylpyridine (98%), Lithium perchlorate (99.9%) were obtained from Macklin.

2.2 Synthesis of urchin-like NiO nanoparticles

NiCl2·6H2O (2.377 g) was dissolved in 20 mL of deionized (DI) water, after which 10 mL of 1 M urea solu tion was added slowly poured under constant mixing for 30 min, after which the mixture was placed into a 100 mL Teflon-lined stainless steel autoclave cup. The hydrothermal reaction was performed at 120 ℃ for 8 h. The formed solids were centrifuged, rinsed with DI water and ethanol several times, dried at 80 ℃ for 12 h, and then annealed at 400 ℃ for 2 h.

2.3 Electrode fabrication

To synthesis NiO photocathodes, the obtained paste was coated on the clean FTO conducting glass (TEC15, 15 V/square, Pilkington, USA) by screen printing, which was remained at 120℃ for 5 min. This step was continued for 6 times. The NiO electrodes were uniformly sintered at 500℃ for 30 min.

Chemical bath deposition (CBD) was used to prepare PbS-QDs sensitized NiO photoelectrode. First, NiO films (fabricated as described in the previous paragraph) were immersed into 0.1 M thioglycolic acid for 1 min, and then into 0.5 M ethanol solution of $Pb(NO_3)_2$ (0.5 M) (also for 1 min). After the samples were dried, they were immersed into 0.5 M Na_2S solution for 1 min and then dried. This step was repeated 1-4 times. The resulting electrodes were marked as "NiO/PbS-N", where N is the number of the cycles. The working NiS electrode was divided with a hot-melt Surlyn 1702 film (25 μm, DuPont). Glass substrate was immersed into 0.5 M $Ni(NO_3)_2$ solution (in ethanol) for 30 s, dried, soaked for 30 s in 0.5 M Na_2S solution (in methanol) and dried. This step was repeated up to 5 times.

2.4 QDSC fabrication

The QDSCs were assembled employing the PbS sensitized NiO photocathode and the NiS counter electrode as well as shelled with the conductive sides facing inward. The polysulfide electrolyte was poured into the joint between two electrodes. The polysulfide electrolyte was composed of 0.01 M tetramethyl ammonium sulfide $((CH_3)_4N)_2S$, 0.02 M 4-tert-butylpyridine (TBP), 0.02 M $LiClO_4$, 0.002 M S, 3-Methoxypro-pionitrile (MPN) was served as a solvent for the polysulfide electrolyte. The $((CH_3)_4N)_2S$ was synthesised by heating tetramethyl ammonium hydroxide $((CH_3)_4N)OH$ and ammonium sulfide $(NH_4)_2S$ at 100℃.

3. OPTICAL AND PHOTOVOLTAIC MEASUREMENTS

Crystallinity and phase compositions were analyzed by X-ray diffraction (XRD) performed using the XD-3A instrument operated using CuKα radiation and a scintillation counter. Sample chemical composition was analyzed by energy dispersive spectroscopy (EDS) coupled with a scanning electron microscope (SEM) fabricated by Oxford Inca. UV-vis absorption spectra were collected using a U-4100 spectrometer (fabricated by HITACHI, Japan). The incident photon-to-current conversion efficiency (IPCE) was measured by a Hypermonolight instrument model SM-25 fabricated using Jasco Co. (Japan). Photocurrent density-voltage measurements were performed at 100 mW/cm^2 incident light intensity using AM 1.5G solar simulator model 16S-002 calibrated using standard Si solar cell and fabricated by SolarLight Co. (USA). Total testing areas of the solar cells as 0.159 cm^2. Linear sweep voltammetry (LSV) was employed to obtain *J-V* curves using an electrochemical workstation model LK9805 fabricated by Lanlike Co. (China). Electrochemical impedance spectroscopy (EIS) was conducted in the dark at -

0.75 V bias using an impedance/gain-phase ZENIUM analyzer fabricated by ZAHNER (Germany). All tests performed using the same electrolyte. The spectra were collected in the 10^{-1}-10^{5} Hz frequency range at room temperature at 10 mV alternate current (AC) amplitude.

4. RESULTS AND DISCUSSION

4.1 SEM analysis and TEM analysis

Scanning Electron Microscope (SEM) and transmission electron microscopy (TEM) images are investigated to display the morphology and structure of NiO nanoparticles (Figure 2a-b) and PbS/NiO composites (Figure 2c-d). As shown in Figure 2a, the urchin-like architecture NiO is obviously observed by the low-magnification SEM image, the diameters of the NiO nanoparticles can be estimated about 1μm. Besides, the SEM image of the high magnification is presented in Figure 2b, which can be observed that each urchin composing numerous nanowires. These nanowires are equally arranged, which have a typical diameter in the range of 20 to 50 nm. Similar observations are made in the TEM images of the samples. The TEM image in Figure 2c presents the morphology of the PbS/NiO composites, which indicates that PbS are successfully deposited on the NiO. The lattice pattern of PbS/NiO composites are declared in the HRTEM image in Figure 2d.

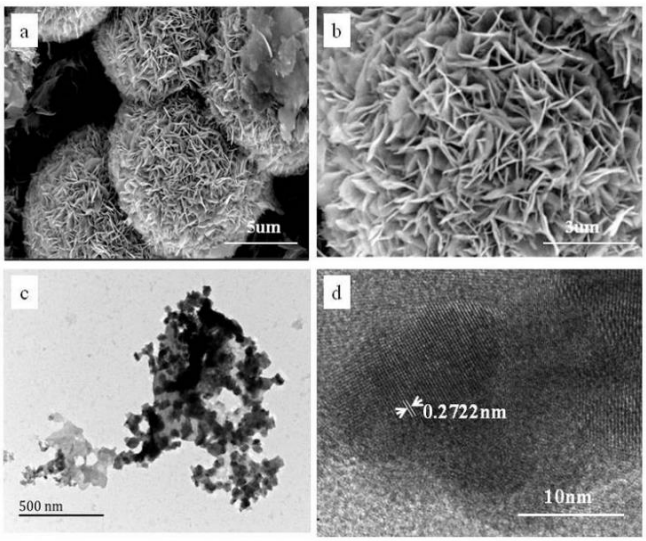

Figure 2. SEM images of NiO nanoparticles (a) low magnification; (b) high magnification; (c) TEM images of PbS/NiO composites (d) the high resolution lattice pattern of PbS/NiO

4.2 XRD analysis

The crystal structures of NiO and the deposited PbS are further characterized by X-ray diffraction (XRD). In the pattern of the pure NiO film reveals a bunsenite phase at 43.16 (200), with other planes (111), (220), (311). All the values are in good agreements according to JCPDS-02-1216. After deposition of PbS Quantum-dots on the surface of NiO thin film, the new diffraction peak is perfectly indexed to scattering from the (111), (200), (220) and (311) planes. Furthermore, the obtained values are in accord with the previously reported data (JCPDS card NO.05-0592), indicating that the PbS is a pure galena phase. The result further confirmes that nanoparticle composites are composed of both well-crystallized PbS nanoparticles and bunsenite NiO. In addition, there are no obvious peaks for impurity on the patterns, which indicates that the sample is pure and no other impurities generated during the process.

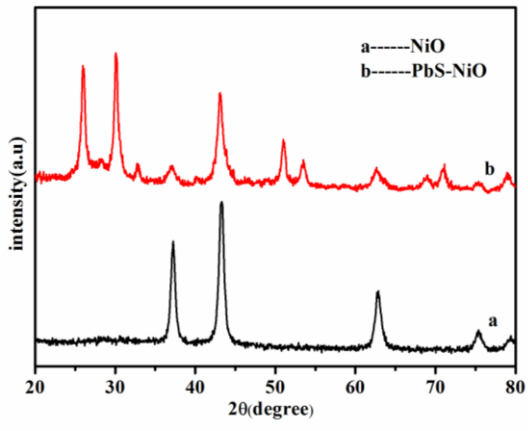

Figure 3. XRD spectra of NiO (a) and NiO/PbS (b)

4.3 Elemental composition

The bulk composition analysis of the PbS deposited NiO are carried out by energy dispersive X-Ray (EDS) spectrometer. As shown in Figure 4, we can clearly see characteristic peaks corresponding to Ni and O elements, deriving from the NiO. The small peak observed for Pb and S demonstrates the existence of Pb and S in the NiO substance. Moreover, the atomic percent of O and Ni was 47.65: 42.46, indicating that the O: Ni ratios is about 1.12:1.0 for NiO. Theoretically, the atomic ratios measured by EDS are relatively closed to their stoichiometries. Therefore, the chemical formulae of the NiO can be expressed according to their stoichiometric ratios. Similarly, the atomic percent of S and Pb is 5.01: 4.88, demonstrating that the S: Pb ratios is nearly 1.03:1.0 for PbS, the same conclusion can be seen according to the aromic percent of Pb and S. The result shows that a successfully deposition of PbS layer covers the NiO surface with a small amount.

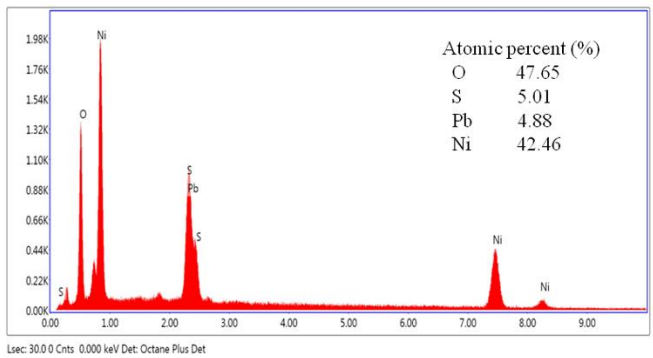

Figure 4. EDS analysis of PbS/NiO nanocomposite

4.4 UV-Vis absorption spectra

UV-Vis absorption spectra of pure and PbS-modified NiO films showed color change and absorbance increase as number

of PbO deposition cycles increased (see Figure 5) from 0 to 4. The UV-Vis absorption spectra of NiO mesoporous film and PbS QDs deposited NiO mesoporous film. For the procedure displayed on the NiO mesoporous film, the thickness of PbS QDs deposition is large, as suggested by the observation of a color change in the film and the higher absorbance of the NiO/PbS electrode. It is clearly noticed that the absorbance is increased when CBD cycles increased, and the absorption shoulder also shows an obvious red shift compare to absorbance onset. The PbS/NiO material absorbance shoulder became red-shifted as number of PbO CBD cycles increased. Absorption wavelength of NiO/PbS-4 and pure NiO film immersed in ((CH3)4N)2S/((CH3)4N)2Sn electrolyte was in the 490-550 nm range, which is beneficial for light capture and enhanced photoelectric efficiency.

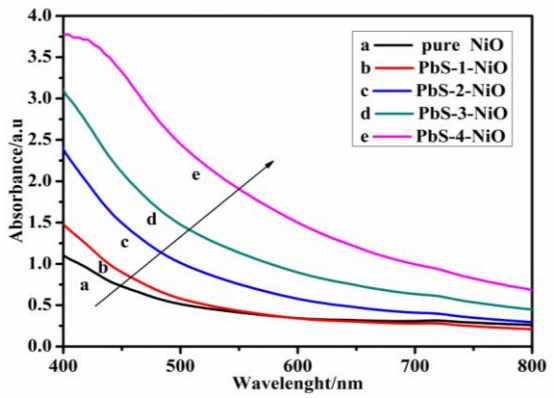

Figure 5. UV-vis absorption spectra of pure and PbS-modified NiO films fabricated using different number of CBD cycles

4.5 J-V characteristics

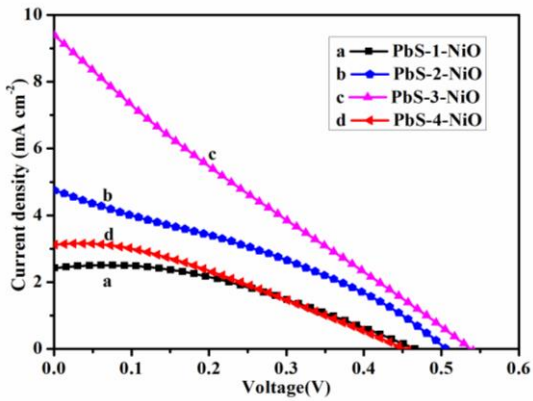

Figure 6. The J-V data obtained for pure and PbS-modified NiO films obtained using different number of CBD cycles. Measurements were conducted under solar light illumination (AM 1.5, 100 mW cm^{-2})

Table 2. Photovoltaic performance of the QDSCs containing NiO/PbS-N (N = 1-4) materials under illumination by the solar light. Areas of all cells were 0.159 cm2.

Sample ID	Cell area (cm^2)	V_{oc}(V)	J_{sc} (mA cm^{-2})	FF	Eff/ %
NiO/PbS-1	0.159	0.467	2.20	0.41	0.42
NiO/PbS-2	0.159	0.507	4.31	0.33	0.73
NiO/PbS-3	0.159	0.538	8.53	0.23	1.07
NiO/PbS-4	0.159	0.454	2.84	0.34	0.44

Figure 6 and Table 2 demonstrate the current density-photovoltage (J-V) data for QDSCs fabricated using NiO/PbS as active material.

As the number of CBD cycles increased from one to three, both short-circuit current density (Jsc) and open-circuit voltage (Voc) increased from 2.20 mA/cm2 and 0.467 V to 8.53 mA/cm2 and 0.538 V, respectively. A maximum PCE value of 1.07% was obtained by the electrode containing PbS-3-NiO as active material. Thus, PbS thickness obtained after three CBD cycles was the best because it provided the highest number of excited electrons capable to improve QDSC photocurrent. After three CBD cycles, PbS layer became too thick for efficient electron injection an excitation mostly because of increased number of recombination in. This also indicates that a thick PbS nanoparticles layer will hinder the regeneration of PbS by the polysulfide electrolyte and enlarge the rate of the recombination reaction.

4.6 IPCE spectrum

IPCE spectra of p-type QDSCs containing PbS/NiO-N composites as active materials (shown in Figure 7) had the same shapes as corresponding absorption spectra. Thus, the photocurrents were generated because of the hole injection from the photo-excited PbS to NiO. The IPCE response for the PbS/NiO-3 material was the largest. The maximum IPCE response of the sensitized NiO was 49% at 340 nm. Such high IPCE value is reported for the first time for the p-type QDSCs. IPCE response could not be simply enhanced by increasing the PbS layer thickness because it eventually led to either inefficient hole injection or overall carrier recombination.

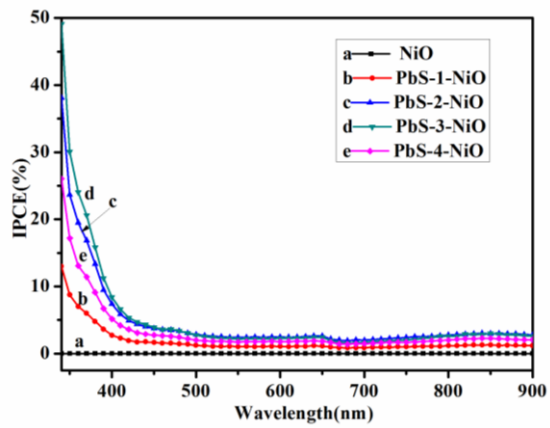

Figure 7. IPCE of pure and PbS-modified NiO films fabricated using 1-4 CBD cycles

4.7 EIS spectrum

EIS data of an electrode containing NiO/PbS-3 film in comparison with EIS for Pt and pure NiS electrode are shown in Figure. 8. EIS parameters were obtained a Z-view software (as shown in Figure 8 and Table 3). In the high-frequency domain, the curve intercept with the real axis is equal to the ohmic series resistance (Rs) of the substrate. The left semicircle in the middle frequency domain represents the charge-transfer resistance (Rct) at the electrode-electrolyte interface. A semicircle in a low-frequency domain reflects the impedance due to the Nernst diffusion (ZN) of the charged species in an electrolyte. Rs value of the pure NiS electrode was 18.1 Ω/cm^2, which was less than that of the Pt-electrode

(which was equal to 27.4 Ω/cm^2). This indicates a strong interaction between the Pt CE and surface sulfide species (e.g., S2-, Sn2-). Rct value directly correlated to the CE catalytic activity, determined by the semicircle radius.35 The Rct values of Pt and NiS CEs were to 3.27 and 1.42 Ω/cm^2, respectively. Small Rct value for NiS CEs indicates its excellent catalytic activity towards ((CH3)4N)2S/((CH3)4N)2Sn reduction because Rct varies inversely proportional to the CE electrocatalytic activity. The ZN values fo rPt and NiS electrodes were 11.75 and 5.64 Ω/cm^2, respectively. Thus, NiS CE had better catalytic activity than Pt CE, which would translate into better photovoltaic performance.

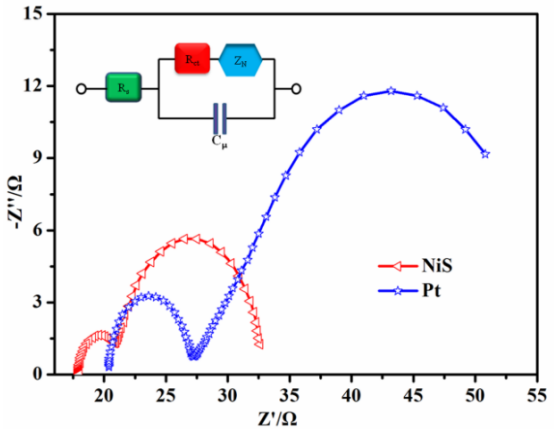

Figure 8. Nyquist plots of the sacrificial cells. Insert shows an equivalent circuit diagram used to fit EIS data

Table 3. Rs, Rct and ZN (all in Ω/cm^2) values for CE cells

CEs	R_s(Ω/cm^2)	R_{ct}(Ω/cm^2)	Z_N(Ω/cm^2)
NiS	18.1	1.42	5.64
Pt	27.4	3.27	11.75

5. CONCLUSIONS

We successfully synthesized NiO films with urchin-like morphology using a high-temperature hydrothermal method. PbS was deposited on NiO film using the CBD process. NiO/PbS composites with different PbS thicknesses were performed. Thickness was varied by a different number of the CBD cycles. The resulting composites were then used as active materials for QDSC photoanodes. Yield (Voc), ff, Jsc, and the cell efficiency values of the solar cell containing PbS/NiO composite fabricated using three CBD cycles were 0.538 V, 0.23%, 8.53 mA cm^{-2}, and 1.07%, respectively. The IPCE value of this electrode was 49% at 340 nm. This is the better IPCE value reported in the literature for p-type QDSCs. Thus, PbS sensitized urchin-like NiO structures are excellent candidates as photocathode active material to produce very efficient p-type solar cells.

ACKNOWLEDGMENT

We gratefully acknowledge the financial support from the following sources: Supported by President Foundation of Hebei University (Grant No.: XZJJ201918).

REFERENCES

[1] Holtzer, M.E., Holtzer, A. (1995). The use of spectral decomposition via the convex constraint algorithm in interpreting the CD-observed unfolding transitions of C coils. Biopolymers: Original Research on Biomolecules, 36(3): 365-379. https://doi.org/10.1002/bip.360360310

[2] Kamat, P.V. (2008). Quantum dot solar cells. Semiconductor nanocrystals as light harvesters. The Journal of Physical Chemistry C, 112(48): 18737-18753. https://doi.org/10.1021/jp806791s

[3] Mora-Sero, I., Giménez, S., Fabregat-Santiago, F., Gómez, R., Shen, Q., Toyoda, T., Bisquert, J. (2009). Recombination in quantum dot sensitized solar cells. Accounts of Chemical Research, 42(11): 1848-1857. https://doi.org/10.1021/ar900134d.

[4] Nozik, A.J., Beard, M.C., Luther, J.M., Law, M., Ellingson, R.J., Johnson, J.C. (2010). Semiconductor quantum dots and quantum dot arrays and applications of multiple exciton generation to third-generation photovoltaic solar cells. Chemical Reviews, 110(11): 6873-6890. https://doi.org/10.1021/cr900289f

[5] Yella, A., Lee, H.W., Tsao, H.N., Yi, C., Chandiran, A. K., Nazeeruddin, M.K., Diau, E.W., Yeh, C.Y., Zakeeruddin, S.M., Grätzel, M. (2011). Porphyrin-sensitized solar cells with cobalt (II/III)–based redox electrolyte exceed 12 percent efficiency. Science, 334(6056): 629-634. https://doi.org/10.1126/science.1209688

[6] Anta, J.A., Guillén, E., Tena-Zaera, R. (2012). ZnO-based dye-sensitized solar cells. The Journal of Physical Chemistry C, 116(21): 11413-11425. https://doi.org/10.1021/jp3010025

[7] Chappel, S., Zaban, A. (2002). Nanoporous SnO_2 electrodes for dye-sensitized solar cells: improved cell performance by the synthesis of 18 nm SnO_2 colloids. Solar Energy Materials and Solar Cells, 71(2): 141-152. https://doi.org/10.1016/S0927-0248 (01)00050-2

[8] Santra, P.K., Kamat, P.V. (2012). Mn-doped quantum dot sensitized solar cells: a strategy to boost efficiency over 5%. Journal of the American Chemical Society, 134(5): 2508-2511. https://doi.org/10.1021/ja211224s

[9] Leschkies, K.S., Divakar, R., Basu, J., Enache-Pommer, E., Boercker, J.E., Carter, C.B., Kortshagen, U.R., Norris, D.J., Aydil, E.S. (2007). Photosensitization of ZnO nanowires with CdSe quantum dots for photovoltaic devices. Nano Letters, 7(6): 1793-1798. https://doi.org/10.1021/nl070430o

[10] Gónzalez-Dominguez, J.M., Gonzalez, M., Anson-Casaos, A., Diez-Pascual, A.M., Gomez, M.A., Martinez, M.T. (2011). Effect of various aminated single-walled carbon nanotubes on the epoxy cross-linking reactions. The Journal of Physical Chemistry C, 115(15): 7238-7248. https://doi.org/10.1021/jp110830y

[11] He, J., Lindström, H., Hagfeldt, A., Lindquist, S.E. (1999). Dye-sensitized nanostructured p-type nickel oxide film as a photocathode for a solar cell. The Journal of Physical Chemistry B, 103(42): 8940-8943. https://doi.org/10.1021/jp991681r

[12] Peter, L.M. (2007). Characterization and modeling of dye-sensitized solar cells. The Journal of Physical Chemistry C, 111(18): 6601-6612. https://doi.org/10.1021/jp069058b

[13] Wang, Z., Shakya, A., Gu, J., Lian, S., Maldonado, S. (2013). Sensitization of p-GaP with CdSe quantum dots: Light-stimulated hole injection. Journal of the American Chemical Society, 135(25): 9275-9278. https://doi.org/10.1021/ja403701p

[14] Kang, S.H., Zhu, K., Neale, N.R., Frank, A.J. (2011). Hole transport in sensitized CdS–NiO nanoparticle photocathodes. Chemical Communications, 47(37): 10419-10421. https://doi.org/10.1039/C1CC13932K

[15] Rhee, J.H., Lee, Y.H., Bera, P., Seok, S.I. (2009). Cu2S-deposited mesoporous NiO photocathode for a solar cell. Chemical Physics Letters, 477(4-6): 345-348. https://doi.org/10.1016/j.cplett.2009.07.014

[16] Bachmeier, A., Hall, S., Ragsdale, S.W., Armstrong, F.A. (2014). Selective Visible-Light-Driven CO_2 Reduction on a p-Type Dye-Sensitized NiO Photocathode. Journal of the American Chemical Society, 136(39): 13518-13521. https://doi.org/10.1021/ja506998b

[17] He, J., Lindstrom, H., Hagfeldt, A., Lindquist, S.E. (2000). Dye-sensitized nanostructured tandem cell-first demonstrated cell with a dye-sensitized photocathode. Solar Energy Materials and Solar Cells, 62(3): 265-273. https://doi.org/10.1016/S0927-0248(99)00168-3

[18] Safari-Alamuti, F., Jennings, J.R., Hossain, M.A., Yung, L.Y.L., Wang, Q. (2013). Conformal growth of nanocrystalline CdX (X= S, Se) on mesoscopic NiO and their photoelectrochemical properties. Physical Chemistry Chemical Physics, 15(13): 4767-4774. https://doi.org/10.1039/C3CP43613F

[19] Mori, S., Fukuda, S., Sumikura, S., Takeda, Y., Tamaki, Y., Suzuki, E., Abe, T. (2008). Charge-transfer processes in dye-sensitized NiO solar cells. The Journal of Physical Chemistry C, 112(41): 16134-16139. https://doi.org/10.1021/jp803919b

[20] Li, L., Gibson, E.A., Qin, P., Boschloo, G., Gorlov, M., Hagfeldt, A., Sun, L. (2010). Double-layered NiO photocathodes for p‐type DSSCs with record IPCE. Advanced Materials, 22(15): 1759-1762. https://doi.org/10.1002/adma.200903151

[21] Lu, Q., Li, L., Xiao, J., Sui, H., Li, J., Duan, R., Li, J., Zhang, W., Li, X., Yang, K., Zhang, Y., Wu, M. (2017). Assembly of CdS nanoparticles on boron and fluoride co-doped TiO_2 nanofilm for solar energy conversion applications. RSC Advances, 7(46): 29065-29070. https://doi.10.1039/C7RA03071A

[22] Sullivan, I., Zoellner, B., Maggard, P.A. (2016). Copper (I)-based p-type oxides for photoelectrochemical and photovoltaic solar energy conversion. Chemistry of Materials, 28(17): 5999-6016. http://doi.org/10.1021/acs.chemmater.6b00926

[23] Chen, H.M., Chen, C.K., Chang, Y.C., Tsai, C.W., Liu, R.S., Hu, S.F., Chang, W.S., Chen, K.H. (2010). Quantum dot monolayer sensitized ZnO nanowire-array photoelectrodes: true efficiency for water splitting. Angewandte Chemie International Edition, 49(34): 5966-5969. https://doi.org/10.1002/ange.201001827

[24] Yu, W.W., Qu, L., Guo, W., Peng, X. (2003). Experimental determination of the extinction coefficient of CdTe, CdSe, and CdS nanocrystals. Chemistry of Materials, 15(14): 2854-2860. http://doi.org/10.1021/cm033007z

[25] Bolton, J., Bailey, T.S., Rzayev, J. (2011). Large pore size nanoporous materials from the self-assembly of asymmetric bottlebrush block copolymers. Nano Letters, 11(3): 998-1001. https://doi.10.1021/nl103747m

[26] Wang, P., Wang, L., Ma, B., Li, B., Qiu, Y. (2006). TiO_2 surface modification and characterization with nanosized PbS in dye-sensitized solar cells. The Journal of Physical Chemistry B, 110(29): 14406-14409. https://doi.org/10.1021/jp060390x

[27] Rhee, J.H., Lee, Y.H., Bera, P., Seok, S.I. (2009). Cu2S-deposited mesoporous NiO photocathode for a solar cell. Chemical Physics Letters, 477(4-6): 345-348. https://doi.org/10.1016/j.cplett.2009.07.014

[28] Raissi, M., Pellegrin, Y., Jobic, S., Boujtita, M., Odobel, F. (2016). Infra-red photoresponse of mesoscopic NiO-based solar cells sensitized with PbS quantum dot. Scientific Reports, 6(1): 1-7. https://doi.org/10.1038/srep24908

[29] Wang, R., Li, Q., Xie, D., Xiao, H., Lu, H. (2013). Synthesis of NiO using pine as template and adsorption performance for Pb (II) from aqueous solution. Applied Surface Science, 279: 129-136. https://doi.org/10.1016/j.apsusc.2013.04.049

[30] Zheng, K., Žídek, K., Abdellah, M., Zhang, W., Chábera, P., Lenngren, N., Yartsev, A., Pullerits, T. (2014). Ultrafast charge transfer from CdSe quantum dots to p-type NiO: hole injection vs hole trapping. The Journal of Physical Chemistry C, 118(32): 18462-18471. https://doi.org/10.1021/jp506963q

[31] Magrini, A., Lazzari, S., Marenco, L., Guazzi, G. (2017). A procedure to evaluate the most suitable integrated solutions for increasing energy performance of the building's envelope, avoiding moisture problems. International Journal of Heat and Technology, 35(4): 689-699. https://doi.org/10.18280/ijht.350401

[32] Hariharan, G., Moorthi, N.S.V., Karthickeyan, D., Thanikaikarasan, S. (2019). Influence of annealing temperature on the characteristics of chemical bath deposited zinc sulphide thin films for solar cell applications. Journal of New Materials for Electrochemical Systems, 22(1): 1-4. https://doi.org/10.14447/jnmes.v22i1.a01

[33] Santra, P.K., Kamat, P.V. (2012). Mn-doped quantum dot sensitized solar cells: A strategy to boost efficiency over 5%. Journal of the American Chemical Society, 134(5): 2508-2511. https://doi.org/10.1021/ja211224s

[34] Gónzalez-Dominguez, J.M., Gonzalez, M., Anson-Casaos, A., Diez-Pascual, A.M., Gomez, M.A., Martinez, M.T. (2011). Effect of various aminated single-walled carbon nanotubes on the epoxy cross-linking reactions. The Journal of Physical Chemistry C, 115(15): 7238-7248. https://doi.10.1021/jp110830y

[35] Takahashi, Y., Kobayashi, Y., Wang, Z., Ito, Y., Ota, M., Ida, H., Kumatani, A., Miyazawa, K., Fujita, T., Shiku, H., Korchev, Y.E., Miyata, Y., Fukuma, T., Chen, M., Matsue, T. (2020). High-resolution electrochemical mapping of the hydrogen evolution reaction on transition-metal dichalcogenide nanosheets. Angewandte Chemie-International Edition, 59(9): 3601-3608. https://doi.org/10.1002/anie.201912863